Using magnetotransport to determine the spin splitting in graphite

J. M. Schneider,[1,*] N. A. Goncharuk,[2] P. Vašek,[2] P. Svoboda,[2] Z. Výborný,[2] L. Smrčka,[2] M. Orlita,[1] M. Potemski,[1] and D. K. Maude[1]

[1]*Laboratoire National des Champs Magnétiques Intenses, Grenoble High Magnetic Field Laboratory, CNRS, 25 Avenue des Martyrs, 38042 Grenoble, France*

[2]*Institute of Physics, Academy of Science of the Czech Republic, Cukrovarnická 10, 162 53 Prague 6, Czech Republic*

(Received 28 January 2010; published 7 May 2010)

Magnetotransport at low temperatures and high-magnetic fields has been used to probe the spin splitting of the electron and hole Landau bands in natural graphite. Tilting the sample in the magnetic field allows to tune the Zeeman energy and hence the spin splitting. Due to the movement of the Fermi energy in the magnetic field, it is necessary to use the full Slonczewski, Weiss, and McClure Hamiltonian to extract the spin splitting. The effective g factor is found to be $g_s=2.5\pm0.1$ with no measurable anisotropy within experimental error. This value is somewhat larger than the value of the anisotropic g-factor determined using electron spin resonance, which is attributed to the many body contribution to the transport g factor.

DOI: 10.1103/PhysRevB.81.195204 PACS number(s): 71.20.−b, 71.18.+y

I. INTRODUCTION

Graphite consists of sheets of hexagonally arranged carbon atoms which are weakly coupled in the out of plane direction, i.e., parallel to the c axis. Graphite is a semimetal with electron and hole puddles along the $H-K-H$ edge of the hexagonal Brillouin zone.[1] The coupling between the layers leads to a k_z dependent in-plane dispersion relation, where z is the direction perpendicular to the layers. As the interplanar distance is roughly 2.5 times the in-plane carbon-carbon bond length, each layer of carbon atoms can be regarded as being independent. Logically, the electrical conductivity is extremely anisotropic with $\rho_c/\rho_{ab}\approx10^4$ in high-quality crystals so that graphite can be considered as a quasi-two-dimensional (2D) system.[2] Nevertheless, the band structure of graphite has resolutely three dimensional origins. Indeed, the additional degree of freedom provided by the interlayer coupling modifies the Fermi surface topology for the lower Landau bands. The signature of such a topological phase transition, observed recently using the Nernst effect, is exclusive to three dimensions.[3]

In a magnetic field the properties of graphite are remarkably well described by the Slonczewski, Weiss, and McClure (SWM) band structure calculations.[4,5] Shubnikov de Haas, de Haas van Alphen, and thermoelectric measurements which probe the physics at the Fermi energy, have largely confirmed the SWM-model of graphite. While orbital effects have been extensively used to caliper the Fermi surface,[6–12] the more subtle spin effects have received less attention. This is perhaps because the well documented movement of the Fermi energy in a magnetic field seriously complicates the extraction of the spin splitting (g factor) from the magnetotransport data.[7] Recent advances in experimental techniques, in particular the vastly increased desktop computing power available for diagonalizing the SWM Hamiltonian, makes it timely to revisit this problem, extending previous measurements to higher magnetic fields and lower temperatures.

The g factor of graphite has been precisely measured using electron spin resonance (ESR). It is anisotropic, and close to the free electron value[13–16] due to the small spin-orbit coupling of carbon.[17] However, in accordance with Larmor's theorem, electron spin resonance is insensitive to many body effects, and measures the undressed spin splitting corresponding to neutral excitations. Transport techniques on the other hand probe charged spin excitations, which include the exchange interaction due to many body effects. The difference between the electron spin resonance and the transport spin splitting is therefore a measure of the importance of many body effects in graphite.

In this paper, we extend our previous low temperature investigation of natural graphite[12] using tilted magnetic fields up to $B=28$ T in order to probe the spin splitting of the orbital features in the magnetotransport. Since the orbital motion of the carriers depends only on the perpendicular component of the magnetic field, the in plane magnetic field in the tilted configuration can be used to tune the Zeeman energy. The magnetic field splitting, ΔB, of the orbital features due to the spin degree of freedom, does not show the expected quadratic increase as a function of the total magnetic field. This is direct experimental evidence that the Fermi energy is not constant but rather moves in the magnetic field. The magnetotransport data in tilted magnetic fields has been analyzed using the SWM model, including a self-consistent calculation of the Fermi level movement, to extract the spin splitting, and hence the g factor, $g_s=2.5\pm0.1$ for both electrons and holes. The usual simple model which calculates the magnetic field position for the spin Landau bands crossing the Fermi energy can explain the observed ΔB versus total magnetic field dependence provided the movement of the Fermi level, taken from the SWM model, is included. Within experimental error we find no evidence for an anisotropy of the magnetotransport g factor. Nevertheless, this result is consistent with previous measurements since our experimental error is comparable with the reported ESR anisotropy of the g factor.

II. EXPERIMENT

For the measurements mm-size pieces of natural graphite with a thickness of a few hundred microns were used. The

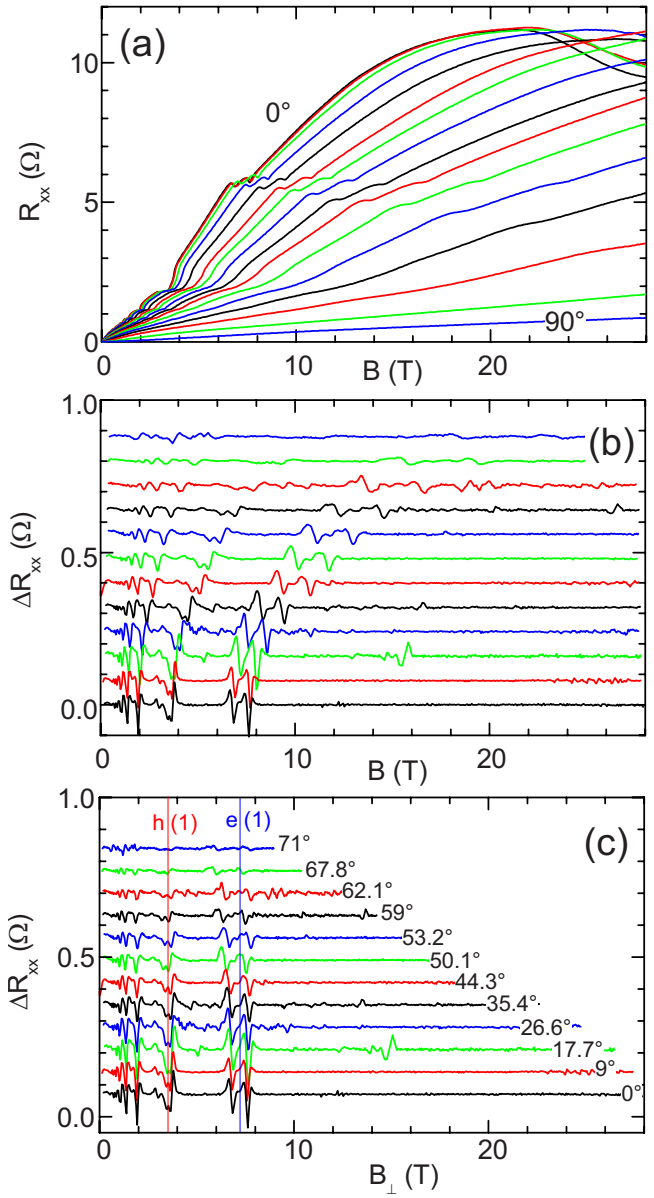

FIG. 1. (Color online) (a) $R_{xx}(B)$ for various orientations of the magnetic field ($0° \leq \theta \leq 90°$) showing the rapid decrease in the amplitude of the magnetoresistance for increasing tilt angles. Quantum oscillations are superimposed on the large magnetoresistance background. (b)-(c) Background removed signal ΔR_{xx} as a function of (b) the total magnetic field and (c) perpendicular magnetic field $B_\perp = B\cos(\theta)$. In (c) the $n=1$ electron and hole features are indicated by vertical solid lines showing that they depends only on $B_\perp$ component of the magnetic field.

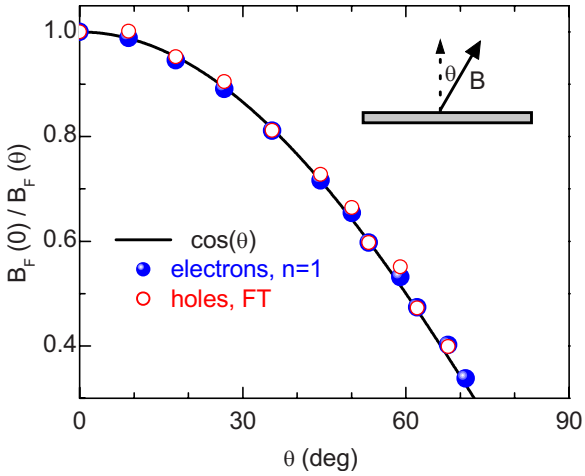

FIG. 2. (Color online) Normalized "fundamental" magnetic field $B_F(\theta=0)/B_F(\theta)$ as a function of the angle for the electron and hole oscillations. Both electrons and holes show a nearly perfect $\cos(\theta)$-dependence (solid line), revealing the large anisotropy of graphite.

silver paint contacts were made in an approximate Hall-bar configuration with the current flowing in the *ab* plane. The measurements were performed using a 28 T resistive magnet and a ^{3}He cryostat ($T \approx 300$ mK), equipped with an *in situ* rotation stage. The longitudinal resistance $R_{xx}(B)$ was measured using conventional phase sensitive detection with a current of 10 μA at 10.7 Hz. The exact orientation of the rotation stage corresponding to $B \| ab$ was determined experimentally by minimizing the magnetoresistance $R_{xx}(B)$ at low-magnetic field.[6] The current through the sample was parallel to the magnetic field for $B \| ab$.

III. RESULTS AND DISCUSSION

A. Angular dependence of the quantum oscillations

The longitudinal resistance R_{xx} as a function of the magnetic field from $B=0-28$ T for various orientations between $\theta=0°$ ($B \perp ab$) and $\theta=90°$ ($B \| ab$) is shown in Fig. 1(a). In perpendicular magnetic field ($\theta=0°$), $R_{xx}(B)$ increases by three orders of magnitude between $B=0$ T and $B=21$ T. Above 21T the resistance decreases signaling the onset of a charge density wave state.[18–20] In the magnetic field range $0<B<8$ T, small quantum oscillations due to the majority electrons and holes Fermi surfaces are superimposed on the large magnetoresistance background.[7–12] When the sample is tilted away from $B \perp ab$, the magnetoresistance is strongly suppressed, which is a clear signature of the highly anisotropic nature of the carrier transport in graphite. Nevertheless, the magnetoresistance for $\theta=90°$ remains considerable. It is only one order of magnitude smaller than for $\theta=0°$. However, this could be attributed to a small residual $B \perp ab$ component of the magnetic field if the sample was slightly misaligned on the rotation stage preventing the $\theta=90°$ condition ever being reached. Comparing the $\theta=0°$ and the $\theta=90°$ data curves, we estimate that an experimentally plausible misalignment of $\simeq 2.7°$ would be sufficient to explain the observed magnetoresistance. Additionally, the lack of crystal perfection, e.g., the possible misalignment of layers within the sample, should be considered.[21]

For increasing tilt angles the quantum oscillations are shifted to higher (total) magnetic field. The quantum oscillations are better seen in the background removed data ΔR_{xx} [see Fig. 1(b)]. Here the large magnetoresistance background is removed by subtracting a smoothed (moving window average) data curve. A Fourier transformation of ΔR_{xx} versus

$(1/B)$ with the magnetic field applied perpendicular to the sample plane, gives fundamental frequencies of B_F=6.15 T and B_F=4.50 T for electrons and holes, respectively. In Fig. 1(c) ΔR_{xx} is shown as a function of the perpendicular magnetic field $B_\perp = B\cos(\theta)$. Plotted in this way there is no shift of the magnetic field position of the quantum oscillations with the tilt angle showing that their position depends only on the perpendicular component of the magnetic field. Thus, the orbital motion of the carriers is effectively confined within the *ab* plane (each graphene sheet) due to the extremely anisotropic conductivity in graphite.[2]

This quasi-2D behavior is confirmed in Fig. 2 where we plot the ratio of the "fundamental" frequencies for the holes and the electrons $B_F(0)/B_F(\theta)$ as a function of the tilt angle θ. For the holes the fundamental frequency is obtained from the Fourier transformation at each angle of the corresponding ΔR_{xx} versus $(1/B)$ curve. For the electrons we use rather the position of the $n=1$ feature since the smaller amplitude of the electron oscillations at high-tilt angles makes the Fourier transform unreliable. For both electrons and holes, for angles up to $\theta=70°$, $B_F(0)/B_F(\theta)$ shows a nearly perfect $\cos(\theta)$ dependence, indicated by the solid line. The quasi-2D behavior can be explained by the extreme anisotropy of graphite, i.e., the in–plane coupling is much bigger than the out of plane coupling $(\rho_c \gg \rho_{ab})$.[2] This means that the carrier motion is confined to the plane so that the cyclotron energy depends only on the perpendicular component of the magnetic field $B_\perp$. Nevertheless, the system is not strictly 2D and the weak coupling between the layers gives rise to Landau bands rather then Landau levels. The oscillations in $R_{xx}(B)$ appear when the Landau bands "cross" the Fermi energy (when there is a maximum in the density of states at E_f). Whereas the angle dependence of quantum oscillations has been extensively studied,[6,8,22,23] there has been, to the best of our knowledge, no detailed study of the spin-splitting of the Landau bands.

B. Spin splitting

At very low temperatures $T \simeq 10$ mK, both the electron and hole features are spin split for magnetic fields $B_\perp > 1$ T.[12] At the higher temperatures used here ($T \approx 300$ mK) spin splitting is resolved only for the high-magnetic field $n=1$ electron and hole features. Rotating the sample in field can be used to extract the g factor since the spin splitting depends on the total magnetic field, while the energy of the Landau band depends only on the perpendicular component of the magnetic field. The experimentally observed splitting $\Delta B = B_\downarrow - B_\uparrow$, where $B_\uparrow$ and $B_\downarrow$ are the magnetic field positions of the spin up and spin down features (corresponding to minima in ΔR_{xx}), is plotted as a function of the mean total magnetic field position $B_m = (B_\downarrow + B_\uparrow)/2$ for the $n=1$ electron and hole features in Fig. 3(a). The magnetic field splitting of the $(n=1)$ electron and $(n=1)$ hole features were obtained from the tilted field measurements in Fig. 1(b). For the $n=1$ electron feature ΔB departs significantly from a quadratic behavior $\Delta B \propto B_m^2$ as indicated by the dashed line in Fig. 3(a).

The failure of ΔB to follow a simple quadratic behavior is an experimental signature that the movement of the Fermi

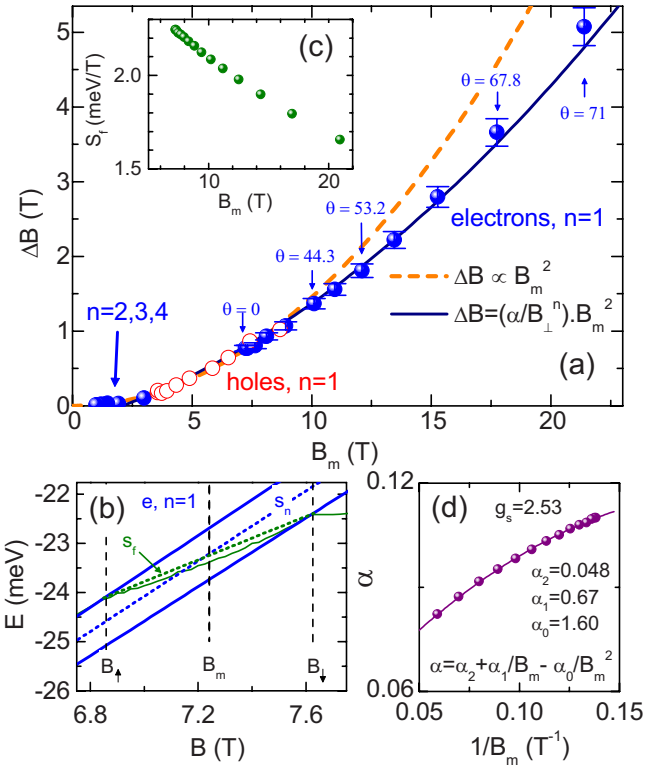

FIG. 3. (Color online) (a) Magnetic field splitting ΔB as a function of the total magnetic field B_m. The broken line is the $\Delta B \propto B_m^2$ dependence (fitted to the low field data) expected if the Fermi energy is constant. The solid line is calculated for the $n=1$ electron Landau band using Eq. (5), which takes into account the movement of the Fermi energy using $g_s=2.53$ (b) Crossing of the $n=1$ electron Landau band with E_f in the $\theta=0$ configuration calculated using the SWM model with $g_s=2.53$ as described in the text. The movement of E_f (solid line), is calculated assuming a constant total electron and hole concentration. The dashed lines indicate linear approximations for S_n and S_f. (c) Magnetic field dependence of S_f obtained from the SWM calculations. (d) Calculated dependence of the parameter $\alpha = g_s\mu_B/(S_n - S_f)$ as a function of $1/B_m$ with $g_s=2.53$. The solid line is fitted using a second-order polynomial.

energy must be taken into account when extracting the g factor. A simple expression can be derived from the crossing points of a given spin up and spin down Landau band and the Fermi energy,

$$\Delta B = \frac{g_s \mu_B B_m}{(S_n - S_f)\cos(\theta)} = \frac{\alpha B_m}{\cos(\theta)}, \tag{1}$$

where $S_n = \Delta E_n/\Delta B_\perp$ is the slope of the n-th Landau band and $S_f = \Delta E_f/\Delta B_\perp$ is the slope of the Fermi energy in the n-th Landau band obtained from the two crossing points as illustrated for the $\theta=0$ configuration in Fig. 3(b). The angle θ can be taken from experiment, however, a simple expression can also be derived,

$$\cos(\theta) = \frac{B_\perp^n + \frac{g_s\mu_B \Delta B}{4(S_n - S_f)}}{B_m} = \frac{B_\perp^n + \frac{\alpha}{4}\Delta B}{B_m}, \tag{2}$$

where $B_\perp^n$ is the perpendicular magnetic field position for the crossing of the (non spin split) n-th Landau band and the

TABLE I. Summary of the SWM tight binding parameters used here.

	(eV)		(eV)
γ_0	3.37 ± 0.02	γ_4	0.07 ± 0.01
γ_1	0.3766 ± 0.05	γ_5	0.05 ± 0.01
γ_2	-0.025 ± 0.001	γ_6	-0.007
γ_3	0.31 ± 0.05	E_f	-0.0287

Fermi energy [see Fig. 3(b)]. For both equations we have a single independent dimensionless fitting parameter $\alpha = g_s \mu_B / (S_n - S_f)$. Thus, to extract the g factor it is necessary to know both S_n and S_f. In addition, any analysis which neglects the movement of the Fermi energy ($S_f = 0$) will overestimate the g factor. Eliminating $\cos(\theta)$ from Eqs. (1) and (2) gives,

$$\Delta B = \frac{\alpha B_m^2}{B_\perp^n + \frac{\alpha}{4}\Delta B} \approx \frac{\alpha B_m^2}{B_\perp^n}, \tag{3}$$

since $\alpha \ll 1$, so that to a good approximation $B_\perp^n \gg \frac{\alpha}{4}\Delta B$. Equation (2) shows that the experimentally accessible B_m has some physical significance since $B_m \cos(\theta) \simeq B_\perp^n$ to a good approximation. This also implies that Eq. (2) should not be used to extract the g factor since the shift in the perpendicular magnetic field value of the spin split features ($\frac{\alpha}{4}\Delta B$) is too small to be reliably determined from experiment. Neglecting the movement of the Fermi energy, the model predicts $\Delta B \propto B_m^2$ in contradiction with experiment. The dashed line in Fig. 3(a) is fitted to the $\theta = 0$ data point assuming $\Delta B \propto B_m^2$. It does not well reproduce the data set and also requires, if we assume $S_f = 0$, an unrealistically large g factor ($g_s \approx 6.5$).

The fact that for a given total magnetic field the splitting ΔB of the ($n=1$) hole and electron Landau bands are the same is at first sight surprising since the effective mass for electrons (0.054 m_e) and holes (0.028 m_e) are fundamentally different.[24,25] However, we will see that this is fully consistent with the predictions of the Slonczewski, Weiss, and McClure band structure calculations when the movement of the Fermi energy is included.

C. Slonczewski, Weiss, and McClure model

In order to extract the g factor, we use the SWM band structure model[4,5] with its seven tight binding parameters $\gamma_0, \ldots, \gamma_6$ as described in Ref. 12. For $\gamma_3 \neq 0$, the magnetic field Hamiltonian has infinite order, which was numerically reduced to a 600×600 matrix for the exact diagonalization procedure. Since the orbital motion of the carriers depends only on the perpendicular component of the magnetic field, the effect of the in-plane magnetic field can be incorporated into the SWM model through an effective spin splitting $\Delta_s = g_{\text{eff}} \mu_B B_\perp$ where the real g factor $g_s = g_{\text{eff}} \cos(\theta)$. Note, that the aperiodicity of the magneto oscillations at high-magnetic fields is inherent to the SWM model.[26] In graphite, E_f moves with the applied perpendicular magnetic field as carriers are transferred between the electron and hole pockets.[6] The Fermi level has to be calculated self-consistently assuming

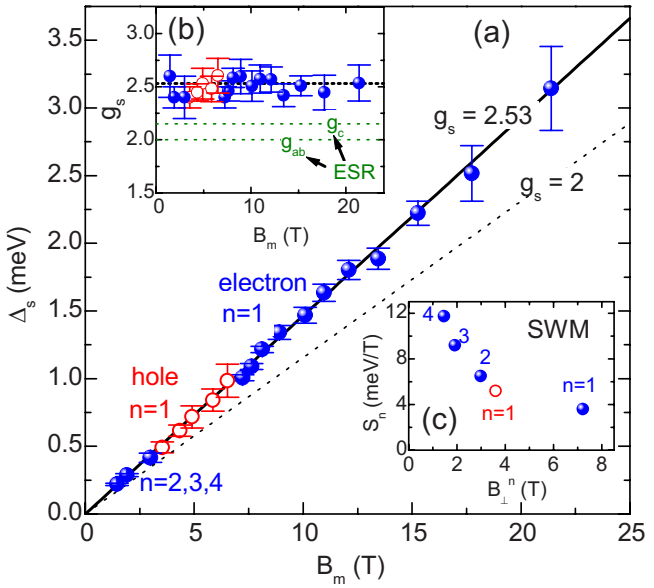

FIG. 4. (Color online) (a) Spin splitting Δ_s for the electron and hole Landau bands, obtained by fitting the SWM model to the data in Fig. 3(a), as a function of the magnetic field. The solid line is a linear fit to the data giving $g_s = 2.53$. The dashed line corresponds to the free electron value of $g_s = 2$. (b) The SWM g factor for each data point in (a). The thick dashed line corresponds to $g_s = 2.53$ while the thin dashed lines correspond to the anisotropic electron spin resonance g factors. (c) SWM calculation of the slope S_n of the electron and hole Landau bands where they cross the Fermi energy as a function of the perpendicular magnetic field component.

the sum of the electron and hole concentrations is constant, $n - p = n_0$. As in Ref. 12, we have used $n_0 = -2.4 \times 10^{17}$ cm^{-3}. At each angle, the effective spin splitting is found for which the SWM model gives the correct magnetic field position for the crossing of the spin up and spin down Landau band with the Fermi energy. Fitting to the spin split high-magnetic field data requires a slight refinement of the SWM parameters, and the values used are given in Table I. Compared to our previous work[12] the changes are small, with the parameters γ_1 and γ_2 changing by only 3%–4%.

Figure 4(a) shows the result for the spin splitting Δ_s extracted from the SWM calculations as a function of the total magnetic field for the $n=1$ hole and the $n=1-4$ electron Landau bands. The data for the $n>1$ electron features, taken from Ref. 12, was measured only for the $\theta = 0$ configuration at $T = 10$ mK. The spin splitting is similar for both the electron and holes Landau bands at a given total magnetic field. Δ_s increases linearly with magnetic field and a linear fit to $\Delta_s = g_s \mu_B B_m$ (solid line) for both electron and hole Landau bands gives $g_s = 2.5 \pm 0.1$. While the value of g_s found here is similar to the value published by *Woollam* a comparison is not really meaningful since in Ref. 7 the SWM parameter γ_3 was neglected.

Alternatively, the g factors calculated from each data point in Fig. 4(a) (using $\Delta_s = g_s \mu_B B_m$) are plotted in Fig. 4(b). Within experimental error there is no magnetic field (angular) dependence of the g factor, which is also consistent with the linearity of Δ_s versus B_m, and justifies *a posteriori*, our neglect the g-factor anisotropy in the analysis. Anisotropy

can be included in our analysis simply by writing $\Delta_s = g_{\text{eff}}\mu_B B_\perp$ where $g_{\text{eff}} = g_c + g_{ab}\tan(\theta)$. However, the scatter in the data [see Fig. 4(b)] is comparable to the anisotropy observed in electron spin resonance measurements. Thus, the anisotropy is too small to be observed in the transport data. A value of $g_s = 2.5 \pm 0.1$ is also consistent with the very simple estimation made from the magnetic field at which spin splitting occurs, ($B_z \sim 1$ T), and at which the Shubnikov de Haas oscillations start ($B_c \sim 0.07$ T) in the perpendicular configuration and at $T = 10$ mK.[12] Assuming the Landau level broadening to be independent of the magnetic field we can write $g_s\mu_B B_z = \hbar e B_c / m^*$ where $m^* = 0.056 m_e$ is the electron effective mass,[27] so that $g_s \approx \hbar e B_c / m^* \mu_B B_z \approx 2.5$.

Electron spin resonance measurements in graphite,[15,16] give a low temperature anisotropic g factor of $g_{ab} = 2.003$ for $B \| ab$ and $g_c = 2.15$ for $B \| c$. These values are close to the free-electron value of $g = 2.0023$ as expected for carbon with its small spin-orbit coupling parameter Λ.[17] In accordance with Larmor's theorem, optical techniques measure the splitting corresponding to neutral ($k = 0$) transitions and are therefore insensitive to many body corrections. Magnetotransport measurements, on the other hand, are sensitive to long wavelength charged excitations which include the many body (Coulomb) contribution to the spin splitting. The significantly larger value of $g_s = 2.5 \pm 0.1$ found here in transport measurements is therefore attributed to the many body (exchange) enhancement of the spin splitting. In two dimensions, the enhanced spin gap can be written,[28]

$$\Delta_s = g\mu_B B_m + \frac{n_\uparrow - n_\downarrow}{n_\uparrow + n_\downarrow}\frac{e^2}{\varepsilon \ell_B}, \tag{4}$$

where g differs from the free electron g factor due to the spin-orbit coupling in graphite and the magnetic length $\ell_B = \sqrt{\hbar / eB_\perp^n}$ depends only on the perpendicular component of magnetic field. This implies that for given Landau band crossing E_f, the Coulomb energy $e^2/\varepsilon \ell_B$ is constant. Therefore, to reproduce the observed linear dependence of $\Delta_s(B_m)$ a linear increase in the spin-polarization $(n_\uparrow - n_\downarrow)/(n_\uparrow + n_\downarrow)$ as a function of B_m is required. To verify this a self-consistent calculation of the spin polarization is required since the spin splitting depends on the polarization and vice versa. However, to a first approximation the spin polarization will vary as $\delta E \cdot D(E_f)$ where $\delta E = g\mu_B \delta B_m$ and $D(E_f)$ is the density of states at the Fermi level, i.e., linearly with the magnetic field.

D. Spin splitting including the movement of the Fermi energy

We can also extract from the SWM model the slope of the Landau bands, which do not depend on the parallel magnetic field component. The slope of the electron and hole Landau bands when they cross the Fermi energy are summarized in Fig. 4(c). The movement of the Fermi energy within the $n = 1$ electron band can be reproduced in a rather simple way based on the results of SWM calculations in the $\theta = 0$ configuration illustrated in Fig. 3(b). The Fermi energy movement within the spin split Landau band can be fitted nearly perfectly by a second-order polynomial. From the SWM calculations, we know that the slope of E_f at $B_\downarrow$ is to a good approximation constant i.e., independent of the spin splitting (angle). Using this fact, the Fermi energy movement for a given angle can be approximated by shifting the $\theta = 0$ second-order polynomial [equivalent to writing the polynomial with coordinates $(B - B_\downarrow)$] and extrapolating the behavior of E_f to lower magnetic fields. The calculated slope of the Fermi energy movement within the $(n = 1)$ electron Landau band is given in the Fig. 3(c). From Eq. (3), it is obvious that it is the magnetic field dependence of S_f, and therefore of α, which leads to the nonquadratic behavior of ΔB as a function of the total magnetic field.

In order to compare the predictions of Eq. (3) with the measured ΔB versus B_m, we need to include the magnetic field (angular) dependence of the dimensionless parameter α. In Fig. 3(d), the calculated value of α is plotted versus the inverse magnetic field for the $n = 1$ electron Landau band. Here, $\alpha = g_s\mu_B B/(S_n - S_f)$ is calculated using $g_s = 2.53$, $S_n = 3.576$ meV/T, and $S_f(B_m)$, extracted from the SWM model. $\alpha(1/B_m)$ is well approximated by a second-order polynomial (solid line) with the coefficients shown in Fig. 3(d). Substituting the second-order polynomial for α in Eq. (3) gives,

$$\Delta B \approx \frac{1}{B_\perp^n}(\alpha_2 B_m^2 + \alpha_1 B_m - \alpha_0). \tag{5}$$

The predicted variation of ΔB versus B_m for the $n = 1$ electron Landau band, calculated using the coefficients $\alpha_0, \alpha_1, \alpha_2$ given in Fig. 3(d) is indicated by the solid line in Fig. 3(a). The agreement between the data and the simple model is remarkable confirming our hypothesis that the observed deviation from the simple $\Delta B \propto B_m^2$ dependence is due to the movement of the Fermi energy, which in turn leads to a magnetic field (angular) dependence of the dimensionless parameter α.

IV. CONCLUSION

Magnetotransport measurements have been analyzed using the full Slonczewski, Weiss, and McClure band structure calculations for graphite in a magnetic field. Using tilted magnetic fields to tune the Zeeman energy, we extract an effective g factor $g_s = 2.5 \pm 0.1$ for both the electron and hole Landau bands. This is significant larger than the g factor obtained using electron spin resonance showing the importance of many body effects in graphite.

ACKNOWLEDGMENTS

This work has been partially supported by ANR (Contract No. PNANO-019-06 and Projects No. KAN400100652 and No. LC510) and by the collaboration PHC Barrande (Grant No. 19535NF) and MEB (Grant No. 020928).

*johannes.schneider@grenoble.cnrs.fr

[1] P. R. Wallace, Phys. Rev. **71**, 622 (1947).
[2] N. B. Brandt, S. M. Chudinov, and Ya. G. Ponomarev, *Semimetals I. Graphite and its Compounds* (Elsevier, Amsterdam, 1988), and references therein.
[3] Z. Zhu, H. Yang, B. Fauqué, Y. Kopelevich, and K. Behnia, Nat. Phys. **6**, 26 (2010).
[4] J. C. Slonczewski and P. R. Weiss, Phys. Rev. **109**, 272 (1958).
[5] J. W. McClure, Phys. Rev. **119**, 606 (1960).
[6] D. E. Soule, J. W. McClure, and L. B. Smith, Phys. Rev. **134**, A453 (1964).
[7] J. A. Woollam, Phys. Rev. Lett. **25**, 810 (1970).
[8] J. A. Woollam, Phys. Rev. B **3**, 1148 (1971).
[9] J. A. Woollam, Phys. Rev. B **4**, 3393 (1971).
[10] I. A. Luk'yanchuk and Y. Kopelevich, Phys. Rev. Lett. **93**, 166402 (2004).
[11] I. A. Luk'yanchuk and Y. Kopelevich, Phys. Rev. Lett. **97**, 256801 (2006).
[12] J. M. Schneider, M. Orlita, M. Potemski, and D. K. Maude, Phys. Rev. Lett. **102**, 166403 (2009).
[13] G. Wagoner, Phys. Rev. **118**, 647 (1960).
[14] K. Kawamura, S. Kaneko, and T. Tsuzuku, J. Phys. Soc. Jpn. **52**, 3936 (1983).
[15] K. Matsubara, T. Tsuzuku, and K. Sugihara, Phys. Rev. B **44**, 11845 (1991).
[16] D. L. Huber, R. R. Urbano, M. S. Sercheli, and C. Rettori, Phys. Rev. B **70**, 125417 (2004).
[17] G. Dresselhaus and M. S. Dresselhaus, Phys. Rev. **140**, A401 (1965).
[18] Y. Iye, P. M. Tedrow, G. Timp, M. Shayegan, M. S. Dresselhaus, G. Dresselhaus, A. Furukawa, and S. Tanuma, Phys. Rev. B **25**, 5478 (1982).
[19] G. Timp, P. D. Dresselhaus, T. C. Chieu, G. Dresselhaus, and Y. Iye, Phys. Rev. B **28**, 7393(R) (1983).
[20] Y. Iye and G. Dresselhaus, Phys. Rev. Lett. **54**, 1182 (1985).
[21] H. Kempa, H. C. Semmelhack, P. Esquinazi, and Y. Kopelevich, Solid State Commun. **125**, 1 (2003).
[22] D. J. Flood, Phys. Lett. A **30**, 178 (1969).
[23] S. J. Williamson, S. Foner, and M. S. Dresselhaus, Phys. Rev. **140**, A1429 (1965).
[24] M. Koshino and T. Ando, Phys. Rev. B **76**, 085425 (2007).
[25] G. Li and E. Y. Andrei, Nat. Phys. **3**, 623 (2007).
[26] L. Smrčka and N. A. Goncharuk, Phys. Rev. B **80**, 073403 (2009).
[27] P. Nozières, Phys. Rev. **109**, 1510 (1958).
[28] T. Ando and Y. Uemura, J. Phys. Soc. Jpn. **37**, 1044 (1974).